CrossMark

RESEARCH PAPER

Viscosity-difference-induced asymmetric selective focusing for large stroke particle separation

Wenchao Xu[1] · Zining Hou[1] · Zhenhua Liu[1] · Zhigang Wu[1,2]

Abstract We developed a new approach for particle separation by introducing viscosity difference of the sheath flows to form an asymmetric focusing of sample particle flow. This approach relies on the high-velocity gradient in the asymmetric focusing of the particle flow to generate a lift force, which plays a dominated role in the particle separation. The larger particles migrate away from the original streamline to the side of the higher relative velocity, while the smaller particles remain close to the streamline. Under high-viscosity (glycerol–water solution) and low-viscosity (PBS) sheath flows, a significant large stroke separation between the smaller (1.0 µm) and larger (9.9 µm) particles was achieved in a sample microfluidic device. We demonstrate that the flow rate and the viscosity difference of the sheath flows have an impact on the interval distance of the particle separation that affects the collected purity and on the focusing distribution of the smaller particles that affects the collected concentration. The interval distance of 293 µm (relative to the channel width: 0.281) and the focusing distribution of 112 µm (relative to the channel width: 0.107) were obtained in the 1042-µm-width separation area of the device. This separation method proposed in our work can potentially be applied to biological and medical applications due to the wide interval distance and the narrow focusing distribution of the particle separation, by easy manufacturing in a simple device.

✉ Zhigang Wu
  Zhigang.Wu@angstrom.uu.se

[1] State Key Laboratory of Digital Manufacturing Equipment and Technology, Huazhong University of Science and Technology, Wuhan 430074, China

[2] Department of Engineering Science, The Ångström Laboratory, Uppsala University, Uppsala, Sweden

1 Introduction

Microfluidics has been attracting significant attention for the past two decades due to its high efficiency, accuracy and low cost, especially for biological and medical applications. Separating target particles from the mixture is one of the classical research fields in microfluidic applications, and it was recently highlighted as a focus issue. A variety of separation methods have been developed based on the differences in the particle properties such as magnetic susceptibility (Seo et al. 2010; Zborowski and Chalmers 2011), dielectric properties (Huang et al. 2002; Vahey and Voldman 2008), optical properties (Huang et al. 2012, 2013; Shah et al. 2009), shape (Beech et al. 2012), deformability (Beech et al. 2012; Hur et al. 2011) and size.

In the above methods, size difference of particles or cell is widely used. In the active methods relying on an external force field (Bhagat et al. 2010; Shields et al. 2015; Wu and Hjort 2009), such as acoustic field, electric field and optoelectronic tweezers can induced to separate particles of different sizes (Gossett et al. 2010). Acoustic radiation force in an acoustic field drives particles to either the pressure nodes or the pressure antinodes of the standing wave, and the strength of the force is related with volume or size (Gossett et al. 2010). The acoustic field manipulates particles to realize focusing (Shi et al. 2008), collection (Agrawal et al. 2013) and separation (Collins et al. 2014; Devendran et al. 2016; Destgeer et al. 2014). Dielectrophoretic force in an electric field manipulates particles or cell, and the force largely depends on size of particles

(Gossett et al. 2010). Using optoelectronic tweezers Ohta et al. (2007) separated HeLa (cervical carcinoma) and Jurkat (acute T cell leukemia) based on cells polarizability and size (Gossett et al. 2010). In the passive methods relying on the channel geometry and inherent hydrodynamic forces, microscale filters (Sethu et al. 2006; Wu and Hjort 2009), pinched flow fraction (PFF) (Takagi et al. 2005; Yamada et al. 2004), hydrophoretic filtration (Yamada et al. 2007), hydrodynamic spreading control (Zhang et al. 2006; Wu et al. 2007), hydrodynamic filtration (Yamada and Seki 2005), deterministic lateral displacement (DLD) (Huang et al. 2004) and inertial separation (Di Carlo et al. 2007; Hansson et al. 2012; Hur et al. 2010; Park et al. 2009) could separate particles of different sizes (Gossett et al. 2010).

In the passive separation methods, inertial separation methods based on the deflection and focusing of particles are widely used due to their simple structures and potential high throughput. The deflection and focusing of the particles were first observed by Segre and Silberberg (1961, 1962). Their experiments showed that the particles in a quadratic flow migrated away from the center of the tube and focused into an annulus. Later, this phenomenon was theoretically explained and summarized (Amini et al. 2014; Ho and Leal 1974; Matas et al. 2004). Ho and Leal (1974) suggested that the lift force was induced by the shear gradient, due to the curvature of the velocity profile, which drove the particle to migrate away from the channel center. Matas et al. analyzed that the balance between the shear-induced and wall-induced lift force determined an equilibrium position between the center and wall of the channel (Amini et al. 2014; Di Carlo 2009; Matas et al. 2004). According to Segre and Silberberg, the different particles have different equilibrium positions, since the two kinds of forces are related to the diameter of the particles (Amini et al. 2014; Di Carlo 2009; Martel and Toner 2014; Zhou and Papautsky 2013). The particle separation based on the different equilibrium positions was obtained in the simple straight channel (Gossett et al. 2012; Hansson et al. 2012). The Dean drag introduced by modifying the channel was added to lift forces exerted on the particles (Guan et al. 2013; Kuntaegowdanahalli et al. 2009; Park et al. 2009). The force balance among these forces determines the inertial focusing behavior (Martel and Toner 2014). In another study, Rubinow and Keller (1961) suggested that the lateral force originating from the rotation of the particle in a uniform flow drove the particle to migrate. Papautsky investigated the dynamics of the migration of particles to the width centers in rectangular channels with different aspect ratios (Zhou and Papautsky 2013) and utilized the rotation-induced lift force, which led the larger particles to migrate to the width centers of the channels faster than smaller particles to achieve the separation (Zhou et al. 2014).

In addition to the above lift forces concerning inertial migration and focusing (Amini et al. 2014), Saffman (1965) suggested that the particle experienced a lift force induced by the shear in a shear flow. When large amount of particles presents, particle migration may be attributed to shear-induced diffusion in concentrated suspensions (Leighton and Acrivos 1987). In Saffman's work, the relative velocity of the particle and the fluid measured on the streamline through the center of the particle, and the velocity gradient had a strong influence on the lift force (Saffman 1965). In common inertial focusing applications, the Saffman lift force was ignored since the force played an important role only near the wall (Martel and Toner 2014; Zhou and Papautsky 2013). The lift force is relative to the a/H (ratio of the particle diameter a to the channel dimension H) and is not generally applicable to inertial systems with $a/H \ll 1$ (Amini et al. 2014). But in some special circumstances, the force must be considered (Amini et al. 2014). For example, when an additional force, such as gravitational or electrophoretic force, acts on a particle and causes the particles to lag behind the fluid, the lift force begins to determine the particle behavior so that the particle migrates toward the channel center (Kim and Yoo 2009). However, that the Saffman lift force plays a dominant role in the particle separation is rarely explored.

In this work, we propose a new inertial separation method which relies on the high-velocity gradient in the accelerated sample flow. When a sample flow is focused and accelerated by two kinds of sheath flows with different viscosity, a relative velocity between the larger particle and fluid is obtained due to the Reynolds number and the Stokes number of the larger particle. Meanwhile, the high-velocity gradient in the sample flow is formed due to the asymmetric velocity of the sheath flows. The lift force induced by the high-velocity gradient plays a dominant role in the particle deflection. The larger particles experience a migration away from the original streamline to the high relative velocity side, while the smaller particles remain close to the original streamline. We demonstrate that smaller (1 µm) and larger (9.9 µm) particles can be clearly separated. To observe the effect of the sheath flows on the particle separation, we examined the interval distance between the smaller and larger particles and the distribution of the smaller particles under the different flow rates and the different viscosity differences of the sheath flows.

2 Principle

2.1 Dimensionless numbers

The flow characteristics of the fluid and dynamics of the particle motion in the accelerated fluid are analyzed by

dimensionless numbers. The Reynolds number (Re) is defined as the ratio of inertial force to viscous force:

$$Re = \frac{U D_h \rho_f}{\eta} \tag{1}$$

where U is the average velocity of the fluid in the channel, ρ_f is the density of the fluid and η is the dynamic viscosity of the fluid. D_h is the hydraulic diameter of the channel, defined as $D_h = 2WH/(W + H)$ with W and H being the width and height of the main branch channel.

When a particle is suspended in the fluid, the dynamic motion is influenced by the inertial and viscous force. The particle Reynolds number (Re_p) that is used to express the particle motion in a channel flow can be defined as:

$$Re_p = Re \frac{a^2}{D_h^2} = \frac{U \rho_f a^2}{D_h \eta} \tag{2}$$

where a is the diameter of the particle. From this equation, a larger particle tends to keep its original flow. It is more difficult to accelerate a larger particle than a smaller particle.

For a particle in the accelerating flow, its Stokes number is used to describe how quickly the particle adjusts to the changes in the surrounding flow. The Stokes number is defined as the ratio between the particle relaxation time (τ_r) and the characteristic time (t_c) of the flow as:

$$St = \frac{\tau_r}{t_c} = \frac{\rho_p a^2/18\mu}{D_h/U} = \frac{\rho_p a^2 U}{18\mu D_h} \tag{3}$$

where ρ_p is the density of the particle, and μ is the kinematic viscosity of the fluid. Following the above equation, a larger St means that the particle needs more time to accelerate when the surrounding fluid is accelerated.

2.2 Particle deflection

The particle deflects from its original streamline when the particle lags behind the fluid in the shear flow (Saffman 1965). Saffman's analysis showed that the particle experienced an inertial lift force induced by the shear. Due to the velocity gradient of the shear flow, the fluid velocity relative to the particle was larger on the non-boundary side than on the wall side in the reference frame of the particle. The asymmetry of the fluid velocity resulted in lower pressure on the non-boundary side where the fluid velocity is higher than the wall side, leading to the particle to migrate away from the wall. In other words, the lift force exerted on the particle arose from the pressure difference of the particle on both sides (Matas et al. 2004; Saffman 1965). The force depended on the velocity gradient of the fluid and on the relative velocity of the particle and the fluid measured

on the streamline through the center of the particle (Saffman 1965).

Due to the high-velocity gradient, the lift force exerted on the particle plays a dominant role in particle separation when the particle lags behind the fluid. The particle in the fluid is accelerated by the viscous force if there is a sudden acceleration in the fluid. With $Re_p \ll 1$, the particle is accelerated to the fluid velocity since the particle flow is dominated by viscous interactions. With $Re_p > 1$, the particle tends to remain at the original flow and lags behind the fluid since the particle flow is mainly influenced by the inertial force. The relative velocity difference of the particle and the fluid measured on the streamline through the center of particle is bigger in the accelerated sample flow than in the sample flow without acceleration due to the particle Stokes number. In addition, the sample flow is in the flow with a high-velocity gradient, which enhances the difference of the fluid velocity relative to the particle on both sides of the particle. The increase in the difference will cause a bigger lift force, which drives the particle to migrate away from the original streamline through the center of the particle. Thus, with proper adjustment of fluid property and flow rate, some particles deflect from the originally carrier fluid while some others may not or may rarely, leading to the separation of different particles. For example, by applying the above idea, the separation of the differently sized particles can be achieved in a flow with a high-velocity gradient. The larger particles have a bigger relative velocity difference between the particle and the fluid measured on the streamline through the center of particle due to the larger values of Re_p and St. The relative velocity difference between both sides of the larger particles is higher than that of the smaller particles due to the diameter size. So a difference in the lift force exerted on the smaller and larger particles appears, which causes the different particle deflections to achieve the particle separation.

Figure 1 illustrates an approach for particle separation based on the high-velocity gradient by introducing a viscosity difference of the sheath flows to form an asymmetric focusing of the sample flow. By using sheath flows, a particle mixture is asymmetrically focused and accelerated, to lead the particles lagging behind the fluid. Meanwhile, the high-velocity gradient is formed due to the viscosity difference of the two sheath flows. Figure 1c shows the schematics of the separation device. In front of the device, three kinds of fluids, particle mixture, low-viscosity and high-viscosity sheath flows, are primed into the channel. The height of the channel in the device used in the experiments is 18 μm. The length and width of the focusing area that represents the channel from the A–A place to the expansion channel are 6 mm and 70 μm, respectively. The A–A place has a distance of 50 μm from sheath channel wall and is
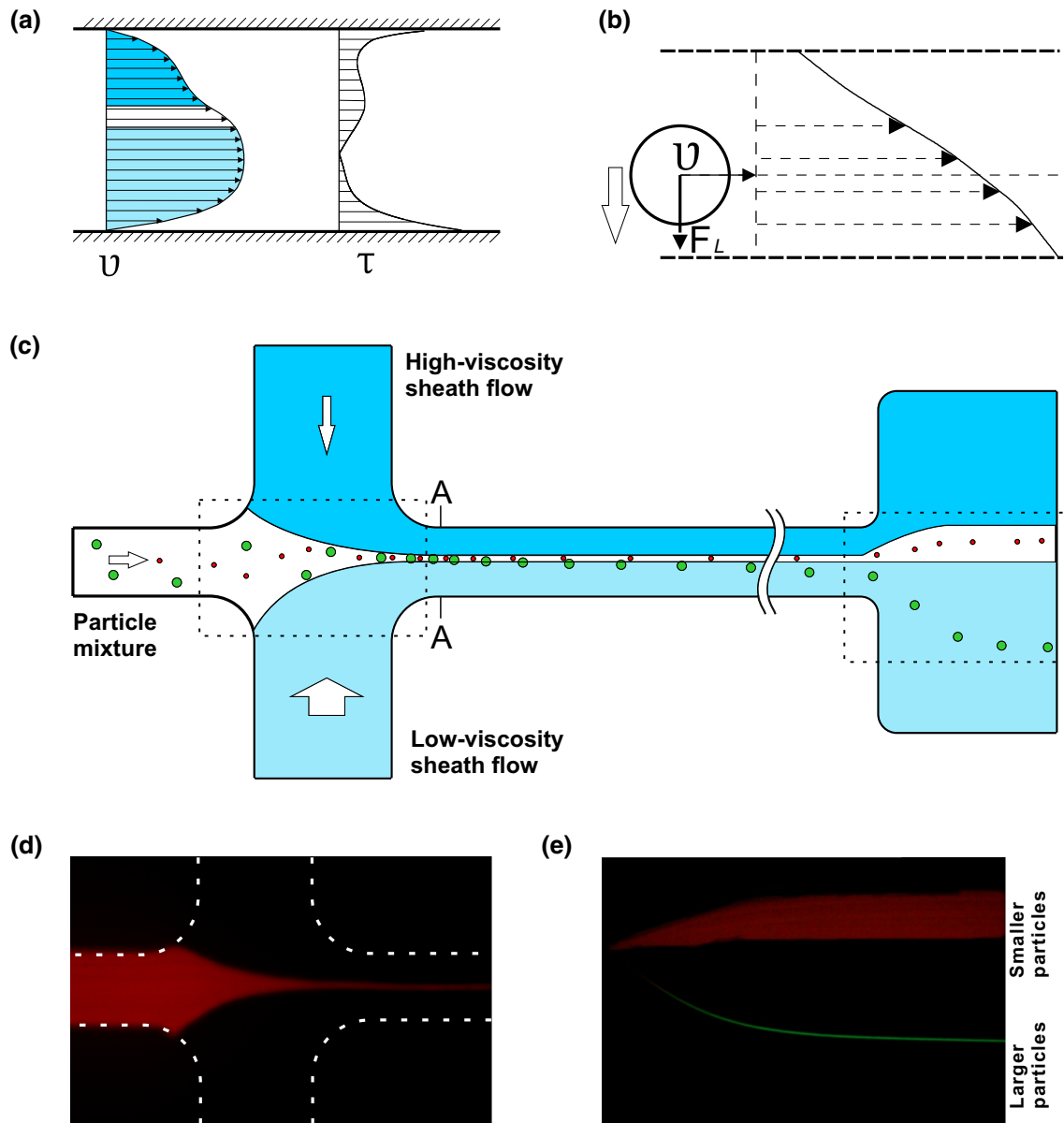
Fig. 1 Mechanism and experimental photographs of particle separation. **a** The fluid velocity profile and shear force at the A–A place of the device; **b** the schematics of the lift force exerted on the particle and the deflection; **c** the schematic illustration of the separation based on viscosity difference of the sheath flow; **d** the experimental photograph of the asymmetric focusing of the particle mixture, the *dotted line* indicates the channel wall; **e** the experimental photograph of the particle separation in the separation area

the place of main channel wall tangent to the transition curve. The width of the separation area that is an expansion channel is 1042 μm. In the focusing area of the device, the larger particles experience a migration away from the original streamline to the low-viscosity sheath flow, while the smaller particles remain close to the original streamline. In the separation area, a large stroke particle separation is achieved.

To identify the high-velocity gradient induced by the viscosity difference, the fluid velocity profile in the A–A place of the focusing area of the device is obtained by using a 3D simulation (COMSOL) as shown in Fig. 1a. In our work, the fluid velocity profiles are all obtained in the plane of the half height of the channel. The velocity profile of the particle mixture is extremely steep. Through the asymmetric focusing, the lift force based on high-velocity gradient plays a dominant role in the particle deflection in Fig. 1b. The particle lagging behind the fluid deflects to the side where the fluid velocity relative to the particle is higher, due to the pressure difference. To directly test the asymmetric focusing and separation of the particle mixture, the focusing area and separation area of the channel are recorded in

Fig. 1d, e, respectively. The two photographs are chosen from particle separation experiment when the ratio of flow rates among the sample flow, the low-viscosity sheath flow (PBS) and the high-viscosity sheath flow (23.5 % (w/w) glycerol–water solution) was 2:4:10 μL min^{-1}.

When the particle lagged behind the fluid, the inertial lift force to drive the particle lateral deflection is given (Saffman 1965) as:

$$F = K\eta\nabla\nu r^2(\gamma/\mu)^{1/2} \qquad (4)$$

where K is a constant, η and μ the dynamic and kinematic viscosity of the fluid, respectively. $\nabla\nu$ is the relative velocity of the particle and the fluid measured on the streamline through the center of the particle, and γ is the shear rate of the particle mixture. However, we have to point out that the equation is only used to infer the relative trend of the lift force since the accurate expression of the inertial lift force for the flow environment in the work has not been found according to our literature survey.

3 Materials and methods

3.1 Materials and chemicals

For the preparation of the device, the silicone (polydimethylsiloxane, PDMS) kit, Elastosil RT601A and B, was supplied by Wacker Chemie (München, Germany). The SU-8 3050 with the corresponding developer was purchased from MicroChem (MA, USA). The 4-inch silicon wafer used as the substrate of standard soft lithography was obtained from Tebo (Harbin, China). Tris (hydroxymethylamino) methane (TRIS) and 2-(4-morpholino)ethanesulfonic acid (MES) and hydroxypropylcellulose (HPC) were all purchased from Alfa Aesar (Karsruhe, Germany) (Wu et al. 2009). A total of 10 % (w/w) Pluronic F-127 (Sigma-Aldrich, St. Louis, USA) was dissolved in ultrapure water (MilliQ, Millipore Corp., USA). Fluorescein disodium dye was purchased from Aladdin (Shanghai, China). For preparation of the particle mixture suspension, two kinds of polystyrene microspheres with diameters 1.0 μm (red fluorescent) and 9.9 μm (green fluorescent) were purchased from Thermo Scientific (MA, USA). The suspension of 1.0 and 9.9 μm particles was mixed at a 1:5 volume ratio and diluted in physiologically buffered saline (PBS) containing 0.1 % (w/w) F-127 to prevent particle adhesion and 1 % (w/w) bovine serum albumin (BSA) to avoid them aggregation at a final concentration of about 1.83×10^8 particles mL^{-1}. Physiologically buffered saline (PBS) was purchased from Basalmedia (Shanghai, China). Bovine serum albumin (BSA) was obtained from Ruji (Shanghai, China). For the preparation of the sheath flow, the low-viscosity fluid adopted was physiologically buffered saline (PBS)

Table 1 Properties of the prepared glycerol–water solution (at 20 °C) in the experiments

Viscosity ratio	Weight fraction (%)	Viscosity (mPa s)
2	23.78	2.01
4	41.60	4.02
8	55.09	8.04

with the viscosity 1.005 mPa s. The high-viscosity fluid was prepared by mixing glycerol (Analytical reagent, Sinopharm, China) with water to match the viscosity, including 2.01, 4.02 and 8.04 mPa s (Sheely 1932). The viscosity ratio was approximately 2, 4 and 8 between the three kinds of glycerol–water solutions and PBS. The properties of the prepared glycerol–water solution (at 20 °C) are listed in Table 1 (Sheely 1932).

3.2 Device fabrication and fluid control

The microfluidic device was fabricated in PDMS using standard soft lithography and bonded to the glass slide by the corona discharger (BD-50E, Electro-Technic Products Inc., IL, USA). The device was filled with 1.5 % HPC dissolved in MES/TRIS buffer (80 mM/40 mM) to avoid particle adhesion to the channel wall after the surface treatment (Wu et al. 2009). The device was then placed overnight in a closed container to maintain a high humidity environment in a refrigerator at 4 °C. The single-use syringe (Gemtier, Shanghai, China) and the polyethylene tubing (NON-TOXIC, PE-20, BD, USA) were coated with 10 % (w/w) F-127 to prevent particle adhesion after the lumen and piston of the single-use syringes were treated by the corona discharger (BD-20V, Electro-Technic Products Inc., IL, USA). The single-use syringes and the tubing were then placed overnight in the same environment as the device. Before particle separation, the device, the single-use syringes and the tubing were flushed with the PBS (Wu et al. 2009). For the experiments, the particle mixture, low-viscosity fluid and high-viscosity fluid were primed into the device by three single-use syringes using three infusion syringe pumps (LSP02-1B, LongerPump, Baoding, China), respectively. The particle motion and fluid flow in the separation system were observed through an inverted fluorescent microscope (Nikon Ti-u, Tokyo, Japan) with a digital SLR camera (Canon EOS 70D, Tokyo, Japan) and a CCD camera (Nikon DS-Qi2, Tokyo, Japan).

3.3 Data acquisition and analysis

In the experiment, a green–red and a blue–green fluorescent attachment were utilized to realize the particle focusing and separation and the fluorescent dye visualization. The digital

Fig. 2 Data acquisition and analysis of particle separation. **a** The experimental photograph of the particle separation in the separation area; **b** the gray level profile of particle trajectories in the separation area of the channel
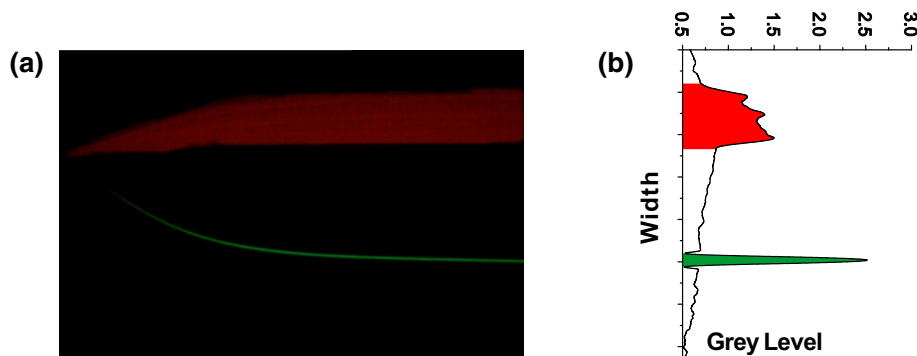
SLR camera was used to record the trajectories of the particle focusing and separation with a 10× objective (NA 0.3) as shown in Fig. 2a. The CCD camera was used to record the focusing of the sample flow containing the fluorescent dye with a 20× objective (NA 0.45). These experimental photographs were collected by using the above recording methods and evaluated by using a self-developed program written in Mathematica (Wolfram Research 10. 2, IL, USA) as shown in Fig. 2b. Through the process, the particle separation can be visualized and the characteristic data of separation can be acquired. The fluid flow in the channel was simulated by using COMSOL (COMSOL Multiphysics 5.1, Stockholm, Sweden) in order to obtain the fluid velocity profile.

4 Results and discussion

4.1 Viscosity-difference-induced asymmetric focusing

The asymmetric focusing as a consequence of the viscosity difference of the sheath flows was visualized by using 0.01 % (w/w) fluorescein disodium dye in PBS as the sample flow. The symmetric and asymmetric focusing photographs recorded by the CCD camera are shown in Fig. 3a, c. Figure 3a shows the focusing of the sample flow with the sheath flows at the same flow rate when 23.5 % (w/w) glycerol–water solution was used as the two kinds of sheath flows. Before our experiments, we have considered adopting glycerol–water solution and sodium alginate solution as the sheath flows. For the glycerol–water solution, it has an effect on cell viability for the biological and medical application in the future, while its viscosity and relationship between viscosity and weight fraction can be easily obtained from other studies such as Sheely's study (1932). For the sodium alginate solution, it has no harm to cell viability and is used to realize the separation of neural cells and glial cells (Wu et al. 2008), while its viscosity and relationship between viscosity and weight fraction cannot be obtained directly according to the literatures.

In order to verify this method of the particle separation and observe the effect of the viscosity difference on this method more directly, we adopt glycerol–water solution as the sheath flows in our work. In fact, the particle separation can be achieved by using sodium alginate solution as the sheath flow, see Section 1 of Supporting Information (SI). The flow rates of the sheath flows were 6 μL min⁻¹. The gray segment indicates the sample flow when the PBS containing fluorescein disodium dye was used as the sample flow. The flow rate of the sample flow was 2 μL min⁻¹. The sheath flows focus the sample flow into the center of the channel. To obtain the fluid velocity profile in the A–A place, a 3D simulation (COMSOL) was used to simulate the fluid flow in the channel as shown in Fig. 3b. The fluid velocity profile was symmetric in the sample flow. The velocity of the sample flow along the channel width tended to have a raise first and then a drop.

The asymmetric focusing was observed with the sheath flows while the two kinds of different viscosity fluid were used as the sheath flows in Fig. 3c. In this group of experiments, PBS was used as the low-viscosity sheath flow and 23.5 % (w/w) glycerol–water solution was still used as the high-viscosity sheath flow. The flow rates of the low-viscosity and high-viscosity sheath flows were 6 μL min⁻¹. The flow rate of the sample flow was 2 μL min⁻¹. The sample flow containing fluorescein salt dye was focused in a narrow lay, which is far away from the channel center. A 3D simulation (COMSOL) revealed that the fluid velocity profile was asymmetric in Fig. 3d. In the profile, the velocity of the focused sample flow gradually increased from the interface between the sample flow and the high-viscosity sheath flow to the interface between the sample flow and the low-viscosity sheath flow. The high-velocity gradient that arises from the steep velocity profile of the sample flow had a monotonous trend according to the definition of the velocity gradient. The relative velocity difference of the fluid to the particle between the both sides of the particle was not zero.

Comparing the two groups of experimental photographs and velocity profiles, we find that the viscosity difference of the sheath flows causes the asymmetric focusing of the
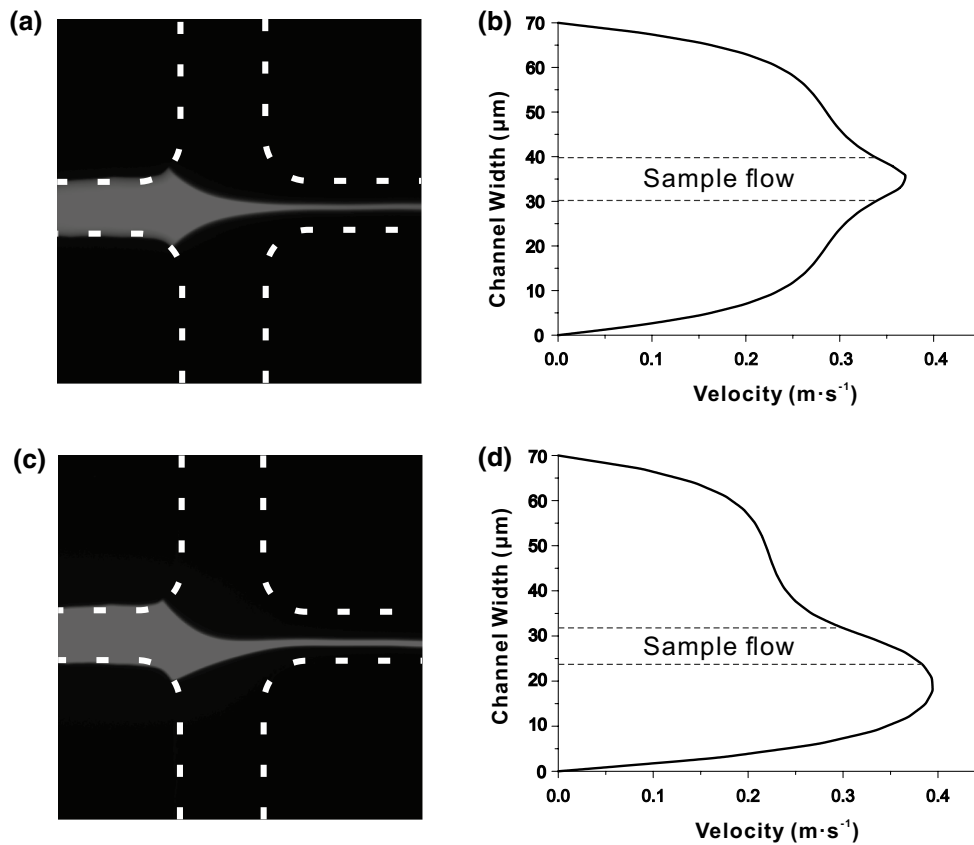
Fig. 3 Comparison of the same and different viscosity sheath flows. **a** The fluorescent visualized the sample flow at the same flow rate and same viscosity of the sheath flow (PBS); **b** the simulation of the velocity profile at the same flow rate and same viscosity of the sheath flow (PBS); **c** the fluorescent visualized the sample flow at high-viscosity (23.5 % (w/w) glycerol–water solution) and low-viscosity (PBS) sheath flows with the same flow rate; **d** the simulation of the velocity profile at high-viscosity (23.5 % (w/w) glycerol–water solution) and low-viscosity (PBS) sheath flows with the same flow rate

sample flow, especially the asymmetric velocity of the sample flow. The high-velocity gradient having a monotonous trend of variation was obtained under the different sheath flow conditions. In order to better observe the variation of the particle deflection and separation in sheath flows with the same and different viscosity, see Section 2 of SI.

4.2 The process of the particle separation in the asymmetric flow

Figure 4 shows the separation process of the different particles according to size in the asymmetric focusing induced by the viscosity difference. The flow rate of the particle mixture, the low-viscosity and high-viscosity sheath flows, were 2, 10 and 4 μL min^{-1}, respectively. The 23.5 % (w/w) glycerol–water solution was used as the high-viscosity fluid. Its viscosity is two times that of the PBS used as the low-viscosity fluid. Four places in the channel are chosen to visualize the separation process. Figure 4a shows the position of the larger and smaller particles in the first place, which is 1 mm away from the A–A place in the

device. Figure 4b shows the profile of fluid velocity at the distance of 1 mm from the A–A place. In Fig. 4b, the red and green bands represent the experimental positions of the smaller and larger particles at the distance of 1 mm from the A–A place. From the figures, we find that the smaller particles are focused in a narrow layer of 6.2 μm width and the center of the larger particles has already deflected from the original streamline. Considering the size of the particles with 1.0 and 9.9 μm, the particles are well separated due to the fact that the center of the larger particles are outside the distribution area of the smaller particles at the time. Figure 4c shows the position of the larger and smaller particles in the second place, which is 2 mm away from the A–A place in the device. Figure 4d shows the profile of fluid velocity at the distance of 2 mm from the A–A place. In Fig. 4d, the red and green bands represent the experimental positions of the smaller and larger particles at the distance of 2 mm from the A–A place. In the figures, the distribution of the smaller particles scarcely changes, but the larger particles have a large distance to the original streamline and an interval has appeared between the
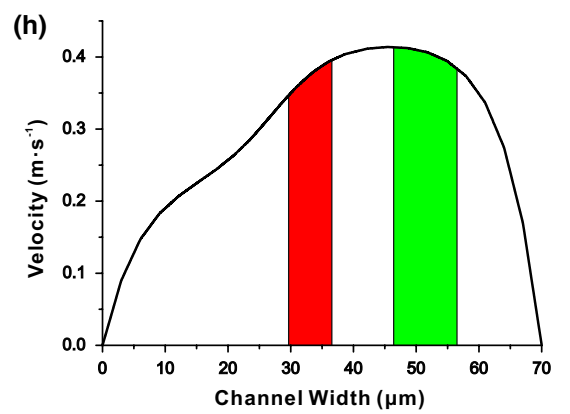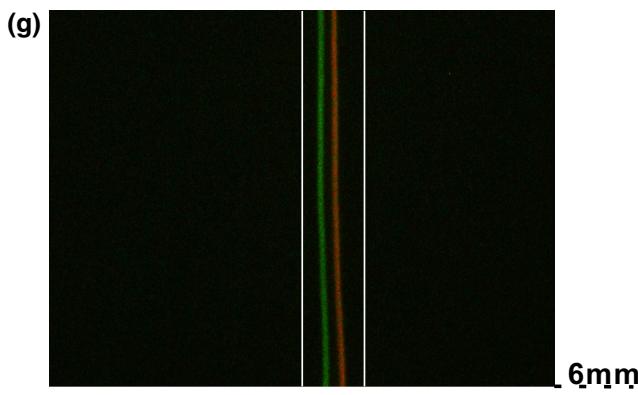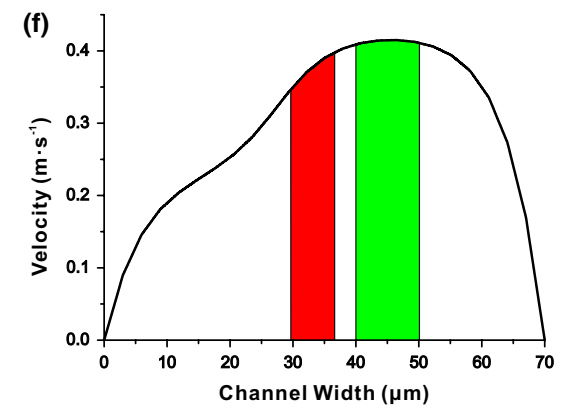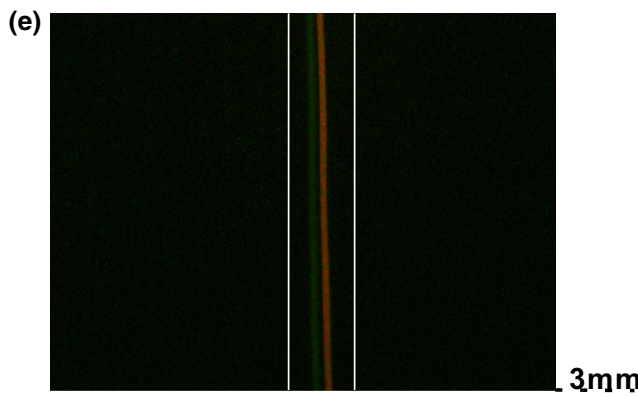
(a)

(b)

1 mm

(c)

(d)

2 mm
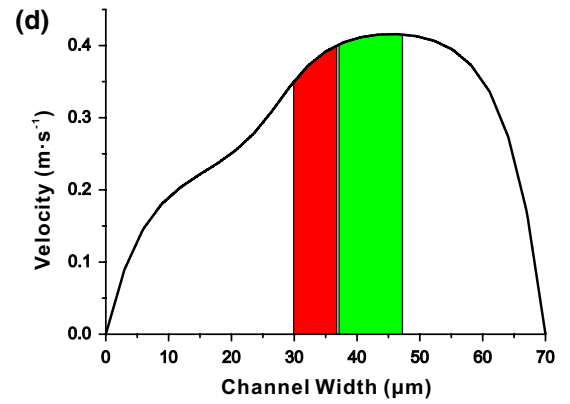
(e)

(f)

3 mm

(g)
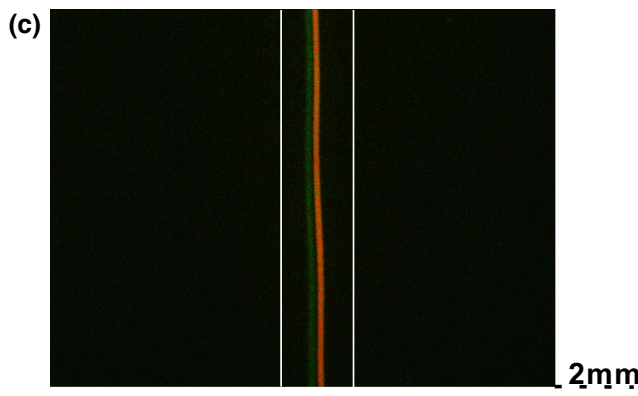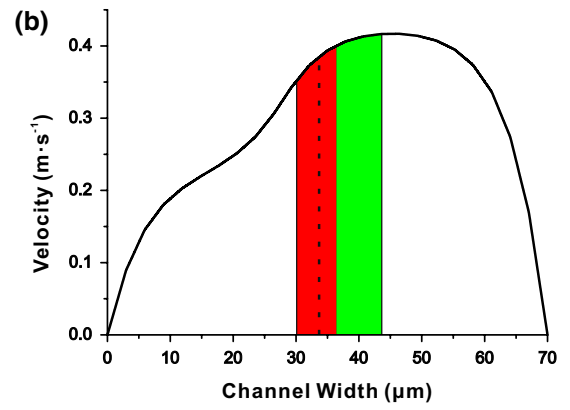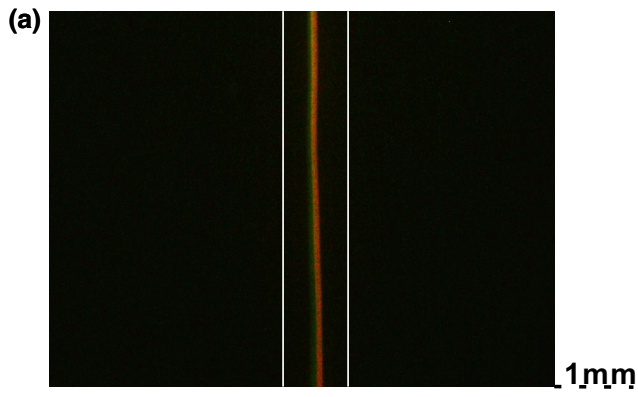
(h)

6 mm

◀**Fig. 4** Process of the particle separation in the focusing area of the channel. **a**, **c**, **e** and **g** the experimental photographs of the smaller and larger particles at a distance of 1, 2, 3 and 6 mm from the A–A place; **b**, **d**, **f**, **h** the experimental positions and velocity profiles of the smaller and larger particles at a distance of 1, 2, 3 and 6 mm from the A–A place

larger and smaller particles. Figure 4e, g shows the position of the larger and smaller particles in the third and fourth place, which is 3 and 6 mm away from the A–A place in the device, respectively. Figure 4f, h shows the profile of fluid velocity at the distance of 3 and 6 mm from the A–A place. In Fig. 4f, h, the red and green bands represent the experimental positions of the smaller and larger particles at the distance of 3 and 6 mm from the A–A place. From the figures, we observe that a big gap appears between the larger and smaller particles, which is helpful in obtaining efficient separation in the channel.

According to Eqs. (2) and (3), the particle Reynolds number and Stokes number of the larger and smaller particle are obtained. The particle Reynolds number (Re_{pl}) of the larger particle was 0.724, and the particle Reynolds number (Re_{ps}) of the smaller particle was 0.00739. The Stokes number (St_l) of the larger particle was 42.3, and the Stokes number (St_s) of the smaller particle was 0.431. With the $Re_{ps} \ll 1$, the smaller particle flow is dominated by viscous interactions. In the process of acceleration, the smaller particles are accelerated to the local fluid velocity due to the viscous drag of the fluid. The lift force exerted on the smaller particle is zero according to Eq. (4). Following Fig. 4a–h, we observe that the smaller particles keep focusing and scarcely deflect, while the larger particles, with the $St_l > 1$, lag behind the fluid as they are not able to respond to the fluid change. The lift force exerted on the larger particles cannot be ignored. The larger particles driven by the force gradually migrate away from their original streamline. Then, they pass through the peak of the fluid velocity and come to the side close to the channel wall in the low-viscosity fluid. In the process, with the larger particles continuously deflecting and smaller staying, their gap gradually increases in the device to realize the separation of particles with different sizes.

4.3 The effect of flow rate between the sheath flows

Figure 5 shows the effect of the flow rate between the sheath flows on the fluid velocity and the particle deflection. The sample flow rate, Q_s, was fixed at 2 µL min^{-1}. The PBS was used as the low-viscosity flow. The flow rate of low-viscosity flow, Q_l, was varied from 1 to 20 µL min^{-1}. The 23.5 % (w/w) glycerol–water solution was used as the high-viscosity flow. The flow rate of the high-viscosity flow, Q_h, was 2, 4 and 8 µL min^{-1},

respectively. The viscosity ratio of the high-viscosity flow to the low-viscosity flow is two. To observe the effect of the flow rate, the high-viscosity flow rate was fixed at $Q_h = 2$, 4 and 8 µL min^{-1}, while the low-viscosity flow rate was varied from 1 to 20 µL min^{-1}. To illustrate the variation of the fluid velocity with the increase in the low-viscosity flow rate, the change of the fluid velocity profile was calculated by using 3D simulation (COMSOL) for two different flow rates between sheath flows when the flow rate of sample flow was 2 µL min^{-1}. The profile of fluid velocity at the distance of 6 mm from the A–A place is shown in Fig. 5a. In the figure, the red and green bands represent the experimental positions of the smaller and larger particles at the distance of 6 mm from the A–A place. The velocity difference of the sheath flows increases, and the velocity profile of the sample becomes steeper with the increase in the low-viscosity flow rate. The variation of the fluid velocity has an influence on the separation and the distribution of the particles. The particle trajectories with the gray level profile visualize the separation and the distribution of the particles as shown in Fig. 2b. To identify the particle trajectories, the low-viscosity flow rate was fixed at $Q_l = 10$ µL min^{-1} while the high-viscosity flow rate was varied from 2 to 8 µL min^{-1}. These three groups of gray level profiles are used as an illustration in Fig. 5b. In the figure, a wide and clear interval appears between the smaller and larger particles. However, at a low flow rate of the low-viscosity flow, the particles in which the smaller and larger particles are not separated overlaps. The two peaks in the gray level may not be in the same position, so the distance (d_d) of the interval was measured to evaluate the separation efficiency of the particles. Figure 5c shows the distance (d_d) of the interval during the varying flow rate of the low-viscosity flow and high-viscosity flow. A clear trend toward an increase can be observed with the increase in Q_l. The distance (d_d) has an effect on the purity of the particle separation. The concentration of the particle separation is related to the focusing and distribution of the particles. From Fig. 5a, we find that the focusing width of the smaller particles changes significantly but none of the larger particles. To evaluate the high concentration of the particle separation, the distribution width (w_d) of the smaller particles in the separation area was measured. Figure 5d shows the variation of the distribution width (w_d) during the varying flow rate of the low-viscosity and high-viscosity flows. The distribution width (w_d) has a clear trend toward a decrease with the increase in Q_l.

In the experiments, the particle Reynolds number (Re_{pl}) of the larger particle was 0.226–1.36 and the particle Reynolds number (Re_{ps}) of the smaller particle was 0.00231–0.0138. The Stokes number (St_l) of the larger particle was 13.2–79.23, and the Stokes number (St_s) of the smaller particle was 0.135–0.8. The smaller particles
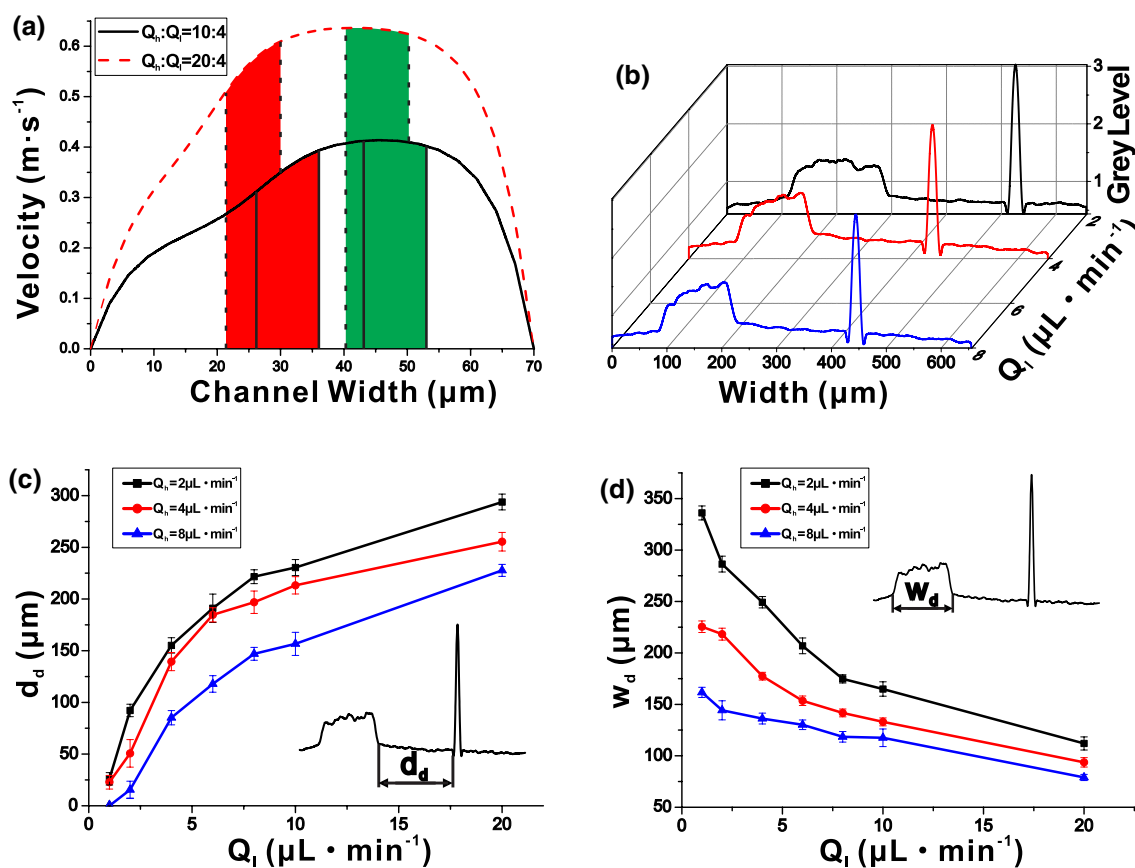
Fig. 5 Simulation of velocity profile and the variation of the interval distance (d_d) and the distribution width (w_d) under different flow rates of the sheath flows. **a** The fluid velocity profile and the position of the particles at two different ratios of low-viscosity sheath flow rate (Q_l) and high-viscosity sheath flow rate (Q_h), and the *red and green bands* represent the experimental positions; **b** the gray level profile of par-ticle trajectories in the separation area of the channel; **c** the interval distance (d_d) between the *smaller* and *larger* particles with different low-viscosity sheath flow rate (Q_l) and high-viscosity sheath flow rate (Q_h); **d** the distribution width (w_d) of the *smaller* particles with differ-ent low-viscosity sheath flow rate (Q_l) and high-viscosity sheath flow rate (Q_h)

with $Re_{ps} \ll 1$ and $St_s < 1$ scarcely migrate away from the original streamline due to the viscous drag of the fluid. The larger particles with $St_l > 1$ are driven by the lift force and experience a migration. So the separation is realized as shown in Fig. 5. Comparing Fig. 5a, c, we find that the flow rate of the sheath flows has an effect on the efficiency of the particle separation. The velocity difference of the par-ticle mixture in Fig. 5a increases with the increase in Q_l while Q_h remains unchanged. With the increase in the dif-ference, the velocity gradient of the larger particle in the particle mixture increases according to the definition of the velocity gradient. Following Eq. (4), the inertial lift force is proportional to the velocity gradient and an increase in the velocity gradient, the inertial lift force increases. Con-sequently, the larger particle driven by the force has a big-ger lateral deflection away from its original streamline with the increase in Q_l. However, the smaller particles still remain at or are close to the original streamline and do not

deflect when $Re_{ps} \ll 1$. So the distance (d_d) increases with the increase in Q_l in Fig. 5c. From the figure, we find that the distance (d_d) decreases with the increase in Q_h. The decrease in the velocity difference in the particle mixture reduces the velocity gradient of the larger particles. The deflection of the larger particle is decreased by the weaken-ing lift force.

Comparing Fig. 5a, d, we find that the flow rate of the sheath flow has an effect on the focusing of the smaller par-ticles. In Fig. 5a, the smaller particles are focused in a nar-rower layer in the straight channel with an increase in Q_l. The distribution width (w_d) becomes narrower in the sepa-ration area of the channel according to the laminar flow in the device. Similarly, with the increase in Q_h, the distribu-tion width (w_d) becomes narrower, as shown in Fig. 5d. The high concentration of smaller particles is collected by prop-erly dividing the fluid. As a result, the increase in the sheath flow rate is helpful in focusing the smaller particles, which
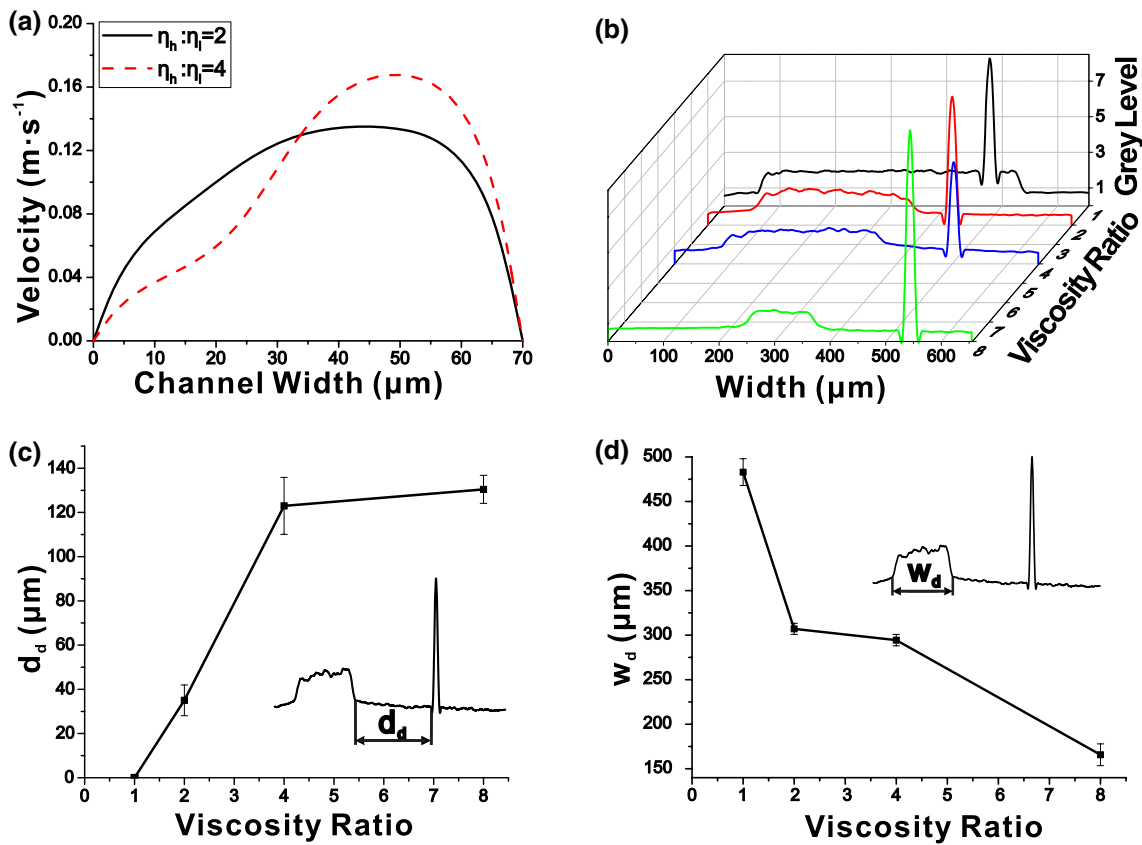
Fig. 6 Simulation of velocity profile and the variation of the interval distance (d_d) and the distribution width (w_d) for different viscosity ratios between sheath flows. **a** The fluid velocity profiles at two different viscosity ratios between the low-viscosity sheath flow (η_l) and the high-viscosity sheath flow (η_h); **b** the gray level profile of particle trajectories in the separation area of the channel; **c** the interval distance (d_d) between the *smaller* and *larger* particles in the separation area of the channel; **d** the distribution width (w_d) of the *smaller* particles in the separation area

has the potential to enhance the collection concentration of the smaller particles in the future.

4.4 The effect of viscosity difference between the sheath flows

Figure 6 shows the effect of a viscosity difference between the high-viscosity and low-viscosity sheath flows on the fluid and the particle deflection. In the experiments, the effect was observed when the high-viscosity sheath flow was changed and the ratio of flow rates of three kinds of flows was fixed. Four groups of different viscosity ratios were tested, which are 1, 2, 4 and 8, respectively. The PBS was used as the low-viscosity sheath flow. The PBS, the 23.5 % (w/w), 48.6 % (w/w) and 56.7 % (w/w) glycerol–water solution were used as the high-viscosity sheath flow in turn. The Q_s:Q_l:Q_h was maintained at 2: 2.5: 1 μL min^{-1}.

To observe the effect of the viscosity difference on the fluid velocity, a profile of the fluid velocity at the distance of 6 mm from the A–A place was adapted by using 3D simulation (COMSOL) in Fig. 6a. The velocity of the high-viscosity flow decreased, while the velocity of low-viscosity flow increased with a rise of the viscosity difference, which raised the asymmetry of the fluid velocity. The velocity gradient of the particle mixture increased with the rise of the asymmetry. To visualize the effect of the viscosity difference on the particle deflection, the particle trajectories with the gray level profile in the separation area of the channel are shown in Fig. 6b. From the figure, we clearly observe that the particle deflection changes with a rise of the viscosity difference. To observe the effect of viscosity difference on the particle deflection, we measured the distance (d_w) of the interval between the smaller and larger particles in Fig. 6c. The distance (d_w) had a clear tendency to increase with a rise of the viscosity difference. The distribution of the smaller particles is measured and presented in Fig. 6d. When the viscosity ratio is 1, the sheath flows and the sample flow have identical viscosity since the PBS was used as the three kinds of flows.

From Fig. 6b, c, we find that the interval distance is zero, while the PBS is both used as high-viscosity sheath flow and low-viscosity sheath flow. In other words, the smaller and larger particles are not obviously separated under these conditions. With the same flow rate, however, the particles are separated when two kinds of the fluid with different viscosity are used as high-viscosity sheath flow and low-viscosity sheath flow.

In the experiments, the particle Reynolds number (Re_{pl}) of the larger particle was 0.245 and the particle Reynolds number (Re_{ps}) of the smaller particle was 0.00254, which was much smaller than 1. The Stokes number (St_l) of the larger particle was 14.5, which was larger than 1, and the Stokes number (St_s) of the smaller particle was 0.148. Comparing Fig. 6a, c, we find the influence of the viscosity difference on the deflection of particles with different size. From Fig. 6a, we see that the fluid velocity of one side close to the high-viscosity flow decreases, but the fluid velocity of the other side close to the low-viscosity flow increases on the both sides of the particle mixture when the rise of the viscosity difference. The change causes the increase in the velocity gradient. From Eq. 4, the force exerted on the larger particles increases, which causes a particle deflection from their original streamlines. However, for the smaller particles still follow their original streamlines due to the $Re_p \ll 1$. When a smaller particle is still in its original streamline of the particle mixture, the bigger deflection of the larger particle driven by the inertial lift force causes the increase in the distance (d_d) in Fig. 6c.

Comparing Fig. 6a, d, we find that a viscosity difference influences the focusing of the smaller particles. From Fig. 6a, the smaller particles are focused by the sheath flows. The viscosity difference of the sheath flows makes the focusing distribution of the particle mixture change and improves the focusing of the smaller particles. When the focusing area of the smaller particles in the straight channel becomes narrower, the distribution width in the separation area becomes smaller due to the laminar feature in the device.

5 Conclusions

We have proposed asymmetric particle separation by introducing sheath flows of different viscosity. The asymmetric focusing of the particle mixture is obtained when the fluid with different viscosity is used as sheath flows. The larger particles are driven by the lift force arising from the velocity gradient migrating away from the original streamline and the smaller particles remaining close to the streamline. The results indicate that the flow rate and the viscosity difference of the sheath flows have an effect on the particle separation. In this work, we have demonstrated that this asymmetric particle separation method has a high efficiency on the separation of the particle mixture and the focusing of the smaller particles, which will contribute to achieving the high purity and concentration of target particles in future applications.

References

Agrawal P, Gandhi PS, Neild A (2013) The mechanics of microparticle collection in an open fluid volume undergoing low frequency horizontal vibration. J Appl Phys 114:114904–114914. doi:10.1063/1.4821256

Amini H, Lee W, Di Carlo D (2014) Inertial microfluidic physics. Lab Chip 14:2739–2761. doi:10.1039/C4LC00128A

Beech JP, Holm SH, Adolfsson K, Tegenfeldt JO (2012) Sorting cells by size, shape and deformability. Lab Chip 12:1048–1051. doi:10.1039/C2LC21083E

Bhagat AAS, Bow H, Hou HW, Tan SJ, Han J, Lim CT (2010) Microfluidics for cell separation. Med Biol Eng Comput 48:999–1014. doi:10.1007/s11517-010-0611-4

Collins DJ, Alan T, Neild A (2014) Particle separation using virtual deterministic lateral displacement (vDLD). Lab Chip 14:1595–1603. doi:10.1039/c3lc51367j

Destgeer G, Ha BH, Jung JH, Sung HJ (2014) Submicron separation of microspheres via travelling surface acoustic waves. Lab Chip 14:4665–4672. doi:10.1039/C4LC00868E

Devendran C, Gunasekara NR, Collins DJ, Neild A (2016) Batch process particle separation using surface acoustic waves (SAW): integration of travelling and standing SAW. RSC Adv 6:5856–5864. doi:10.1039/c5ra26965b

Di Carlo D (2009) Inertial microfluidics. Lab Chip 9:3038–3046. doi:10.1039/B912547G

Di Carlo D, Irimia D, Tompkins RG, Toner M (2007) Continuous inertial focusing, ordering, and separation of particles in microchannels. Proc Natl Acad Sci U S A 104:18892–18897. doi:10.1073/pnas.0704958104

Gossett DR, Weaver WM, Mach AJ, Hur SC, Tse HTK, Lee W, Amini H, Di Carlo D (2010) Label-free cell separation and sorting in microfluidic systems. Anal Bioanal Chem 397:3249–3267. doi:10.1007/s00216-010-3721-9

Gossett DR, Tse HTK, Dudani JS, Goda K, Woods TA, Graves SW, Di Carlo D (2012) Inertial manipulation and transfer of microparticles across laminar fluid streams. Small 8:2757–2764. doi:10.1002/smll.201200588

Guan G, Wu L, Bhagat AA, Li Z, Chen PC, Chao S, Ong CJ, Han J (2013) Spiral microchannel with rectangular and trapezoidal cross-sections for size based particle separation. Sci Rep 3:1475. doi:10.1038/srep01475

Hansson J, Karlsson JM, Haraldsson T, Brismar H, van der Wijngaart W, Russom A (2012) Inertial microfluidics in parallel channels for high-throughput applications. Lab Chip 12:4644–4650. doi:10.1039/C2LC40241F

Ho BP, Leal GL (1974) Inertial migration of rigid spheres in two-dimensional unidirectional flows. J Fluid Mech 65:365–400. doi:10.1017/S0022112074001431

Huang Y, Joo S, Duhon M, Heller M, Wallace B, Xu X (2002) Dielectrophoretic cell separation and gene expression profiling on microelectronic chip arrays. Anal Chem 74:3362–3371. doi:10.1021/ac011273v

Huang LR, Cox EC, Austin RH, Sturm JC (2004) Continuous particle separation through deterministic lateral displacement. Science 304:987–990. doi:10.1126/science.1094567

Huang SB, Chen J, Wang J, Yang CL, Wu MH (2012) A new optically-induced dielectrophoretic (ODEP) force-based scheme for effective cell sorting. Int J Electrochem Sci 7:12656–12667

Huang SB, Wu MH, Lin YH, Hsieh CH, Yang CL, Lin HC, Tseng CP, Lee GB (2013) High-purity and label-free isolation of circulating tumor cells (CTCs) in a microfluidic platform by using optically-induced-dielectrophoretic (ODEP) force. Lab Chip 13:1371–1383. doi:10.1039/C3LC41256C

Hur SC, Tse HTK, Di Carlo D (2010) Sheathless inertial cell ordering for extreme throughput flow cytometry. Lab Chip 10:274–280. doi:10.1039/B919495A

Hur SC, Henderson-MacLennan NK, McCabe ERB, Di Carlo D (2011) Deformability-based cell classification and enrichment using inertial microfluidics. Lab Chip 11:912–920. doi:10.1039/C0LC00595A

Kim YW, Yoo JY (2009) Axisymmetric flow focusing of particles in a single microchannel. Lab Chip 9:1043–1045. doi:10.1039/B815286A

Kuntaegowdanahalli SS, Bhagat AAS, Kumar G, Papautsky I (2009) Inertial microfluidics for continuous particle separation in spiral microchannels. Lab Chip 9:2973–2980. doi:10.1039/B908271A

Leighton D, Acrivos A (1987) The shear-induced migration of particles in concentrated suspensions. J Fluid Mech 181:415–439. doi:10.1017/S0022112087002155

Martel JM, Toner M (2014) Inertial focusing in microfluidics. Annu Rev Biomed Eng 16:371–396. doi:10.1146/annurev-bioeng-121813-120704

Matas J-P, Morris JF, Guazzelli E (2004) Lateral forces on a sphere. Oil Gas Sci Technol 59:59–70. doi:10.2516/ogst:2004006

Ohta A, Chiou P, Phan H, Sherwood S, Yang J, Lau A, Hsu H, Jamshidi A, Wu M (2007) Optically controlled cell discriminationand trapping using optoelectronic tweezers. IEEE J Sel Top Quantum Electron 13:235–243. doi:10.1109/JSTQE.2007.893558

Park J-S, Song S-H, Jung H-I (2009) Continuous focusing of microparticles using inertial lift force and vorticity via multi-orifice microfluidic channels. Lab Chip 9:939–948. doi:10.1039/B813952K

Rubinow SI, Keller JB (1961) The transverse force on a spinning sphere moving in a viscous fluid. J Fluid Mech 11:447–459. doi:10.1017/S0022112061000640

Saffman PG (1965) The lift on a small sphere in a slow shear. J Fluid Mech 22:385–400. doi:10.1017/S0022112065000824

Segre G (1961) Radial particle displacements in Poiseuille flow of suspensions. Nature 189:209–210. doi:10.1038/189209a0

Segre G, Silberberg A (1962) Behavior of macroscopic rigid spheres in Poiseuille flow. J Fluid Mech 14:136–157. doi:10.1017/S0022112062001111

Seo H-K, Kim Y-H, Kim H-O, Kim Y-J (2010) Hybrid cell sorters for on-chip cell separation by hydrodynamics and magnetophoresis. J Micromech Microeng 20:095019. doi:10.1088/0960-1317/20/9/095019

Sethu P, Sin A, Toner M (2006) Microfluidic diffusive filter for apheresis (leukapheresis). Lab Chip 6:83–89. doi:10.1039/B512049G

Shah GJ, Ohta AT, Chiou EP-Y, Wu MC (2009) EWOD-driven droplet microfluidic device integrated with optoelectronic tweezers as an automated platform for cellular isolation and analysis. Lab Chip 9:1732–1739. doi:10.1039/B821508A

Sheely ML (1932) Glycerol viscosity tables. Ind Eng Chem Res 24:1060–1064. doi:10.1021/ie50273a022

Shi J, Mao X, Ahmed D, Colletti A, Huang TJ (2008) Focusing microparticles in a microfluidic channel with standing surface acoustic waves (SSAW). Lab Chip 8:221–223. doi:10.1039/B716321E

Shields CW, Reyes CD, Lopez GP (2015) Microfluidic cell sorting: a review of the advances in the separation of cells from debulking to rare cell isolation. Lab Chip 15:1230–1249. doi:10.1039/C4LC01246A

Takagi J, Yamada M, Yasuda M, Seki M (2005) Continuous particle separation in a microchannel having asymmetrically arranged multiple branches. Lab Chip 5:778–784. doi:10.1039/B501885D

Vahey MD, Voldman J (2008) An equilibrium method for continuous-flow cell sorting using dielectrophoresis. Anal Chem 80:3135–3143. doi:10.1021/ac7020568

Wu ZG, Hjort K (2009) Microfluidic hydrodynamic cell separation: a review. Micro Nanosyst 1:181–192. doi:10.2174/1876402910901030181

Wu ZG, Liu AQ, Hjort K (2007) Microfluidic continuous particle/cell separation via electroosmotic-flow-tuned hydrodynamic spreading. J Micromech Microeng 17:1992–1999. doi:10.1088/0960-1317/17/10/010

Wu ZG, Hjort K, Wicher G, Svenningsen ÅF (2008) Microfluidic high viability neural cell separation using viscoelastically tuned hydrodynamic spreading. Biomed Microdevices 10:631–638. doi:10.1007/s10544-008-9174-7

Wu ZG, Willing B, Bjerketorp J, Jansson JK, Hjort K (2009) Soft inertial microfluidics for high throughput separation of bacteria from human blood cells. Lab Chip 9:1193–1199. doi:10.1039/B817611F

Yamada M, Seki M (2005) Hydrodynamic filtration for on-chip particle concentration and classification utilizing microfluidics. Lab Chip 5:1233–1239. doi:10.1039/B509386D

Yamada M, Nakashima M, Seki M (2004) Pinched flow fractionation: continuous size separation of particles utilizing a laminar flow profile in a pinched microchannel. Anal Chem 76:5465–5471. doi:10.1021/ac049863r

Yamada M, Kano K, Tsuda Y, Kobayashi J, Yamato M, Seki M, Okano T (2007) Microfluidic devices for size-dependent separation of liver cells. Biomed Microdevices 9:637–645. doi:10.1007/s10544-007-9055-5

Zborowski M, Chalmers JJ (2011) Rare cell separation and analysis by magnetic sorting. Anal Chem 83:8050–8056. doi:10.1021/ac200550d

Zhang X, Cooper JM, Monaghan PB, Haswell SJ (2006) Continuous flow separation of particles within an asymmetric microfluidic device. Lab Chip 6:561–566. doi:10.1039/B515272K

Zhou J, Papautsky I (2013) Fundamentals of inertial focusing in microchannels. Lab Chip 13:1121–1132. doi:10.1039/C2LC41248A

Zhou J, Giridhar PV, Kasper S, Papautsky I (2014) Modulation of rotation-induced lift force for cell filtration in a low aspect ratio microchannel. Biomicrofluidics 8:044112. doi:10.1063/1.4891599